Structural and mutational analysis of human Ad37 and canine adenovirus 2 fiber heads in complex with the D1 domain of coxsackie and adenovirus receptor.

Elena Seiradake, Hugues Lortat-Jacob, Olivier Billet, Eric J Kremer, Stephen Cusack

THE JOURNAL OF BIOLOGICAL CHEMISTRY VOL. 281, NO. 44, pp. 33704–33716, November 3, 2006

Structural and Mutational Analysis of Human Ad37 and Canine Adenovirus 2 Fiber Heads in Complex with the D1 Domain of Coxsackie and Adenovirus Receptor*

Received for publication, June 2, 2006, and in revised form, August 21, 2006 Published, JBC Papers in Press, August 21, 2006, DOI 10.1074/jbc.M605316200

Elena Seiradake[‡1], **Hugues Lortat-Jacob**[§], **Olivier Billet**[¶‖**2], **Eric J. Kremer**[¶‖**3], **and Stephen Cusack**[‡4]

From the [‡]*Grenoble Outstation, European Molecular Biology Laboratory, Grenoble, France,* [§]*Institut de Biologie Structurale, Unité Mixte de Recherche (UMR) 5075 Commissariat à l'Energie Atomique-CNRS-Université Joseph Fourier, Grenoble, France,* [¶]*Institut de Génétique Moléculaire de Montpellier,* [‖]*CNRS UMR 5535, and* ***Institut Fédératif de Recherche 122, 34293 Montpellier, France*

Adenovirus fibers from most serotypes bind the D1 domain of coxsackie and adenovirus receptor (CAR), although the binding residues are not strictly conserved. To understand this further, we determined the crystal structures of canine adenovirus serotype 2 (CAV-2) and the human adenovirus serotype 37 (HAd37) in complex with human CAR D1 at 2.3 and 1.5 Å resolution, respectively. Structure comparison with the HAd12 fiber head-CAR D1 complex showed that the overall topology of the interaction is conserved but that the interfaces differ in number and identity of interacting residues, shape complementarity, and degree of conformational adaptation. Using surface plasmon resonance, we characterized the binding affinity to CAR D1 of wild type and mutant CAV-2 and HAd37 fiber heads. We found that CAV-2 has the highest affinity but fewest direct interactions, with the reverse being true for HAd37. Moreover, we found that conserved interactions can have a minor contribution, whereas serotype-specific interactions can be essential. These results are discussed in the light of virus evolution and design of adenovirus vectors for gene transfer.

Adenoviruses (Ads)[5] are nonenveloped icosahedral particles (70–90 nm in diameter) containing double-stranded DNA genomes of 28–42 kbp. They have been isolated from a wide variety of vertebrates, including mammals, birds, reptiles, amphibians, and fish (1). The ~50 human Ad serotypes (HAd) (divided into species A–F) lead to serotype-specific respiratory, ocular, and enteric infections that are usually self-limiting diseases in immunocompetent individuals. However, Ad infections are a significant cause of morbidity and mortality in newborns and immunosuppressed individuals (2). Notably, bone marrow and solid organ transplant patients who have severe lymphocytopenia are at the highest risk for Ad-induced disease (3). In addition, there are no drugs currently available that efficiently prevent or treat infections from all HAd serotypes.

The major adenovirus capsid protein is the trimeric hexon, 240 of which form the 20 facets of the icosahedron. The 12 vertices are composed of the penton complex, which comprises the pentameric penton base and the externally projecting trimeric fiber. The fiber has a shaft of variable length with a terminal globular knob or head domain. In most cell types *in vitro*, the fiber head and penton base mediate attachment and entry, respectively. Crystal structures are available of the HAd2 and HAd5 hexons (4, 5); the HAd2 penton base (6); the fiber head domains of HAd2, HAd3, HAd5, HAd12, HAd37, HAd41 (short); and a construct of HAd2 fiber head plus part of its shaft (7–13) (reviewed in Ref. 14). In addition, there are recent high resolution cryoelectron microscopy reconstructions of the entire virus (15, 16). Based on similarities in overall capsid architecture and capsid protein structure, *Adenoviridae* probably share an ancient common ancestor with bacteriophages of the *Tectiviridae* family (17–19).

The initial stages of adenoviral infection, cellular attachment, and internalization have been described as a two-step mechanism. In the best characterized pathway, based on studies using HAd species C serotypes 2 and 5 (HAd2/5), the fiber head first binds to a primary receptor. In the second step, a conserved Arg-Gly-Asp (RGD) motif in the penton base binds to integrins, triggering endocytosis (20). Enteric HAds belonging to subgroup F and also canine adenovirus type 2 (CAV-2) do not possess an RGD motif in the penton base and may use alternative mechanisms to trigger cell entry (21–23). The first primary Ad receptor identified was the immunoglobulin-like coxsackie and adenovirus receptor (CAR) (24, 25), which is a cell adhesion molecule found in tight junctions (26). A variety of representative viruses from human Ad species A and C–F and nonhuman Ads (*e.g.* CAV-2) have been shown to use CAR as a primary receptor (22, 27). In lung epithelial cells, CAR is

* Part of this work was funded by the Association Française contre les Myopathies (AFM) and the Vaincre les Maladies Lysosomales. The costs of publication of this article were defrayed in part by the payment of page charges. This article must therefore be hereby marked "*advertisement*" in accordance with 18 U.S.C. Section 1734 solely to indicate this fact.

The atomic coordinates and structure factors (code 2J12, 2j2j, 2j1k) have been deposited in the Protein Data Bank, Research Collaboratory for Structural Bioinformatics, Rutgers University, New Brunswick, NJ (http://www.rcsb.org/).

[1] Supported by an EU FP6 Marie Curie Early Stage Research Training Fellowship under Contract MEST-CT-2004-504640 ("E-STAR").

[2] An AFM postdoctoral fellow.

[3] An INSERM Director of Research. To whom correspondence may be addressed: IGMM, CNRS UMR 5535, 1919 Route de Mende, 34293 Montpellier, France. Tel.: 33467613672; E-mail: eric.kremer@igmm.cnrs.fr.

[4] To whom correspondence may be addressed: Grenoble Outstation, European Molecular Biology Laboratory, 6 rue Jules Horowitz, BP181, 38042 Grenoble Cedex 9, France. Fax: 33476207199; Tel.: 33476207238; E-mail: cusack@embl-grenoble.fr.

[5] The abbreviations used are: Ad, adenovirus; HAd, human adenovirus serotype; CAR, coxsackie and adenovirus receptor; SPR, surface plasmon resonance; TEV, tobacco etch virus; Bicine, *N*,*N*-bis(2-hydroxyethyl)glycine; r.m.s., root mean square.

located predominantly on the basolateral side of the cells, where it plays a role in cell-cell adhesion, probably via dimerization of the D1 domain (CAR D1) (26, 28, 29). The crystal structure of the HAd12 fiber head in complex with human CAR D1 revealed the binding site at the interface of HAd12 fiber head monomers and highlighted the AB loop as a critical region involved in CAR binding (13). The HAd12 fiber head-CAR D1 binding site overlaps with the CAR D1 dimerization site (30). The fact that the HAd2 fiber head-CAR D1 affinity is 1000-fold higher than the affinity between CAR D1 monomers supports the finding that excess fiber produced during replication disrupts tight junctions by binding to CAR D1, thus promoting the spread of progeny virus (31).

Most species B (*e.g.* HAd3) and some species D viruses (*e.g.* HAd37) do not use CAR as a primary receptor *in vivo* but attach to CD46 (or MCP (membrane cofactor protein), a regulator of complement activation), sialic acids, and/or other primary receptors (12, 32–36). The short fibers of human enteric viruses HAd40 and HAd41 do not bind CAR either. Crystal structures of HAd3 (11) and HAd41 short fiber (10) show that the reason for the inability to bind CAR is different in each case. For HAd3, there are incompatible charged residues in the AB loop, although the main-chain conformation of the loop is otherwise suitable, whereas for HAd41 short fiber, the AB loop has an altered conformation inconsistent with CAR binding (10). Surprisingly, HAd37 virions and recombinant fiber heads bind to CAR in an overlay blot assay, although the virus does not use CAR as a receptor (37). This may be because the HAd37 fiber shaft is too short and rigid to allow efficient binding to cellular CAR when the fiber is attached to the virus (38). Other studies also confirm that the length and flexibility of the fiber shaft is critical in infectivity (39).

In addition to their importance as human pathogens, Ads are promising tools for the development of gene transfer vectors. Because Ad-induced morbidity is relatively species-specific, we and others hypothesized that vectors derived from nonhuman *Adenoviridae* would be more clinically useful than those derived from human serotypes, based, in part, on the potential lack of ubiquitous memory immunity (cellular and humoral) found in humans (40, 41). We therefore began developing vectors derived from CAV-2 (42–46), one of the >50 nonhuman *Adenoviridae* currently identified. We showed that in the central nervous system of several species (including *ex vivo* human tissue), CAV-2 vectors preferentially transduce neurons and lead to an efficient level of axoplasmic transport (45). Helper-dependent CAV-2 vectors (*i.e.* constructs that contain the Ad inverted terminal repeats, packaging domain, and an exogenous expression cassette but are otherwise devoid of all other viral coding sequences (reviewed in Ref. 47)) lead to long term transgene expression in the central nervous system (46) and respiratory tract (48) of immunocompetent rodents without immunosuppression. These data and those from studies using helper-dependent HAd vectors (47) suggest that helper-dependent CAV-2 vectors could be used for the long term treatment of some global neurodegenerative disorders (49, 50).

To gain further insight into the plasticity of the CAR-fiber head interaction and more generally to improve understanding of adenovirus tropism and vector design, we determined two new crystal structures, those of CAV-2 and HAd37 fiber head in complex with human CAR D1. The structures were solved to 2.3 and 1.5 Å resolution, respectively, significantly better than previous fiber head CAR complex structures. We also determined the structure of the CAV-2 fiber head alone at 1.5 Å resolution, which, together with the known structure of unliganded HAd37 fiber head (12), allows assessment of eventual conformational changes upon complex formation. Based on the structures, we analyzed the CAR-binding properties of wild type and mutant HAd37 and CAV-2 fiber heads using surface plasmon resonance (SPR). Together with existing structural information on the HAd12 fiber head in complex with human CAR D1, we present a more complete understanding of the Ad fiber head interaction with CAR D1.

EXPERIMENTAL PROCEDURES

Plasmids and Cloning—Two vectors derived from pAB3 were kindly provided by Mark van Raaij (Universidad de Santiago), both containing the gene coding for residues 15–140 of human CAR D1, one without any tag (pAB3.CAR15–140) and the other with a noncleavable C-terminal His tag (pAB3.CAR15–140H) (30, 51). Delphine Guilligay (EMBL Grenoble Outstation) generously provided a vector derived from pPROEX HTb (Invitrogen) containing a construct of the HAd37 fiber head (residues 177–365), an N-terminal His_6 tag, and a tobacco etch virus (TEV) protease cleavage site (12). A fragment coding for CAV-2 fiber head residues 358–542 was generated by PCR using CAV-2 genomic DNA as template and cloned into a pQE vector (Qiagen) containing a noncleavable N-terminal His_6 tag. The same fragment was cloned into pPROEX HTb, a vector containing an N-terminal His_6 tag and a TEV protease cleavage site. For crystallization, only the CAV-2 fiber head containing the noncleavable His tag was used. All binding assays using SPR were performed exclusively with the second CAV-2 construct (wild type and mutants), after removal of the tag. To simplify the description of the methods, both constructs will be referred to as "CAV-2 fiber head." For CAR D1, only the untagged construct was used for crystallization, and only the His-tagged construct was used for SPR assays. The point mutants for SPR assays were created using the QuikChange site-directed mutagenesis kit as suggested by the manufacturer (Stratagene).

Expression and Purification of Proteins—Fiber head constructs in pPROEX HTb were expressed in *Escherichia coli* strain BL21 Star (DE3) (Invitrogen). The CAV-2 fiber head in pQE was expressed in *E. coli* strain M15 (Qiagen). All proteins were expressed at 37 °C and in the soluble fraction. Cells were resuspended in lysis buffer (20 mM Tris-HCl, pH 7.5, 300 mM NaCl, 20 mM imidazole, Boehringer Complete EDTA-free protease inhibitor mixture) and lysed by sonication. The cell lysate was centrifuged for 30 min at 25,000 × *g*, and the supernatant was loaded on an Ni^{2+}-nitrilotriacetic acid column (Qiagen). Protein bound to the resin was washed with wash buffer (20 mM Tris-HCl, pH 7.5, 300 mM NaCl, 50 mM imidazole) and eluted with elution buffer (20 mM Tris-HCl, pH 7.5, 150 mM NaCl, 500 mM imidazole). To separate the His tag from constructs containing a TEV protease cleavage site, proteins were incubated overnight with 1:100 His-tagged TEV protease at 10 °C. Imid-

azole was removed by dialysis against lysis buffer. Uncleaved protein and TEV protease were removed by binding to a Ni^{2+}-nitrilotriacetic acid resin. Fiber head protein was concentrated to about 5 mg/ml and either used for complex formation with CAR D1 or loaded onto a Superdex200 column (Amersham Biosciences) for further purification and changing of the buffer to 150 mM NaCl, 10 mM HEPES (pH 7.4).

The preparation of periplasmic extract containing His-tagged or untagged CAR D1 was performed as described (30). Briefly, CAR D1 with or without His tag was expressed in *E. coli* strain XL1 blue (Stratagene) at 25 °C. The cell pellet was washed with phosphate-buffered saline (8 g/liter NaCl, 0.2 g/liter KCl, 1.44 g/liter Na_2HPO_4, 0.24 g/liter KH_2PO_4 (pH 7.4)) and then with (200 mM Tris, pH 8.0, 0.5 mM EDTA, 0.5 M sucrose) and finally incubated for 20 min in 150 ml of distilled water to release the periplasmic fraction. Boehringer Complete EDTA-free protease inhibitor mixture was added. For the purification of untagged CAR D1, NaH_2PO_4, Na_2HPO_4, and NH_4SO_4 were added up to the final concentrations of 25 mM, 25 mM, and 1.5 M, respectively. After centrifugation, the supernatant was loaded onto a 75-ml phenyl-Sepharose FF high sub (Amersham Biosciences) and eluted with a linear gradient of 1.5–0.0 M NH_4SO_4 in PE buffer (25 mM NaH_2PO_4, 25 mM Na_2HPO_4, 1 mM EDTA). Fractions containing CAR D1 were dialyzed against crystallization buffer (see below) and concentrated to 10 mg/ml. For the purification of His-tagged CAR D1, NaCl, Tris, pH 7.5, and imidazole were added to the periplasmic extract to final concentrations of 150, 20, and 20 mM, respectively, and the solution was loaded on a Ni^{2+}-nitrilotriacetic acid column. Protein bound to the resin was washed with wash buffer (20 mM Tris-HCl, pH 7.5, 300 mM NaCl, 50 mM imidazole) and eluted with elution buffer (20 mM Tris-HCl, pH 7.5, 150 mM NaCl, 500 mM imidazole). Eluted CAR D1 was concentrated and loaded on a Superdex200 column (Amersham Biosciences). During this step, the buffer was changed to 150 mM NaCl, 10 mM Hepes, pH 7.4.

To form complexes, fiber head and CAR D1 proteins were mixed in an approximate ratio of 1:1 (w/w), incubated for 10 min at 4 °C, and loaded on a Superdex200 column (Amersham Biosciences). During this step, the buffer was changed to crystallization buffer (150 mM NaCl, 20 mM Tris, pH 7.5). The peak fractions containing the complex of CAR D1 and fiber head were pooled and concentrated to 8.5 mg/ml (HAd37 fiber head and CAR D1) or 9 mg/ml (CAV-2 fiber head and CAR D1).

Crystallization, Data Collection, and Processing of HAd37 Fiber Head in Complex with CAR D1—Crystals were obtained at 20 °C in hanging drops containing 1 μl of protein solution and 1 μl of crystallization solution (17% polyethylene glycol 6000, 0.5 M LiCl, 0.1 M Tris, pH 8) and were flash-frozen in the same solution containing 20% glycerol. Diffraction data were collected to 1.5 Å at the European Synchrotron Radiation Facility (ESRF) on beamline ID14-EH1 using an ADSC Q4R detector. Data were integrated and scaled with XDS (52) (space group *I23*). Data statistics are summarized in Table 1. The asymmetric unit contained one fiber head chain (194 residues, 21.7 kDa) and one chain of CAR D1 (138 residues, 15.3 kDa). Molecular replacement was performed with PHASER (53) using chain A of HAd37 fiber head (Protein Data Bank entry 1UXA) (12) and CAR D1 as found in complex with HAd12 fiber head (13) as models.

Crystallization, Data Collection, and Processing of CAV-2 Fiber Head—CAV-2 fiber head was concentrated to 9.5 mg/ml and crystallized at 20 °C in hanging drops containing 2 μl of protein solution and 4 μl of crystallization solution (0.15 M KBr, 30% polyethylene glycol monomethyl-ether 2000). Data were collected on ESRF beamline ID14-EH1 using an ADSC Q4R detector and integrated with MOSFLM (54) (Table 1). Crystals diffracted to 1.5 Å and contained two fiber head trimers (591 residues, 65 kDa each) in the asymmetric unit (space group $P2_1$). Using an HAd2 fiber head model (Protein Data Bank entry 1QHV) (8), a convincing molecular replacement solution was found by PHASER (53). However, the model could not be used directly in refinement or automated model building; therefore, RESOLVE was used in prime-and-switch mode with 6-fold noncrystallographic symmetry (55). The six noncrystallographic symmetry matrices and subunit centers of mass were derived from the molecular replacement model using SUPERPOSE (56). Initial phases from the model (829 residues) were calculated with SFALL and SIGMAA from the CCP4 suite (57), and these were used for automated model building using ARP/wARP (58), which automatically built 1027 of the final 1086 residues modeled in the asymmetric unit.

Crystallization, Data Collection, and Processing of CAV-2 Fiber Head in Complex with CAR D1—Crystals were obtained at 20 °C in hanging drops containing 1 μl of protein solution and 1 μl of crystallization condition 1 (20% polyethylene glycol monomethyl-ether 550, 0.1 M Bicine, pH 9, 0.1 M NaCl) or condition 2 (0.1 M Hepes, pH 7.5, 30% polyethylene glycol 400, 0.2 M $MgCl_2$). Crystals were flash-frozen without adding additional cryoprotectant. Data were collected on ESRF beamline ID14-EH2 using an ADSC Q4R detector (Table 1). Crystals from condition 1 were of space group *I422* ($a = b = 219.9$ Å, $c = 387.5$ Å), diffracted to 2.3 Å, and contained four trimeric complexes (*i.e.* 12 + 12 chains of fiber head + CAR D1) in the asymmetric unit (total 4020 residues, 443.6 kDa). Crystals from condition 2 were of space group *I4* ($a = b = 158.8$ Å, $c = 183.2$ Å), also diffracted to 2.3 Å, and contained two trimeric complexes (*i.e.* 6 + 6 chains of fiber head + CAR D1) in the asymmetric unit. Data were integrated and scaled with XDS (52). Molecular replacement was performed with PHASER (53), initially using the data scaled to space group *I4*. A model of trimeric CAV-2 fiber head (see above) and CAR D1 as found in complex with HAd12 fiber head (chain B in Protein Data Bank entry 1KAC) (13) were used as models. The resulting coordinate file was used for molecular replacement to solve the structure in space group *I422*. The *I422* electron density map was of better quality than that obtained in *I4* and yielded the final model described here.

All models passed through several rounds of refinement using REFMAC (59). COOT (60) was used for the visualization of models and electron density maps and for the superposition of different models. PROCHECK (61) was used to check the geometry of the model. Noncrystallographic symmetry restraints and TLS refinement were used as appropriate, particularly for the CAV-2 fiber head CAR D1 complex structure. Crystallographic refinement statistics are summarized in Table 1.

Buried surface areas were calculated with AREAIMOL (CCP4 suite). Intermolecular contacts at protein-protein interfaces were analyzed with CONTACT (CCP4 suite) and DIMPLOT (62).

SPR Binding Assays—Surface activation, protein immobilization, and binding assays were carried out using a Biacore 3000 SPR (Biacore, St. Quentin en Yveline, France), essentially as described (51). Briefly, flow cells of a Biacore CM4 sensor chip were activated during 10 min with a cross-linking mixture consisting of 0.2 M 1-ethyl-3-(3-dimethyl-aminopropyl)-carbodiimidehydrochloride and 0.05 M *N*-hydroxysuccinimide, after which CAR D1 (25 μg/ml in 10 mM sodium acetate, pH 5.0) was injected. Different amounts of immobilized protein were obtained by varying the injected volume. Remaining activated groups were blocked with a 10-min pulse of 1 M ethanolamine, pH 8.5. A second flow cell was activated with the cross-linking mixture and immediately blocked with ethanolamine to serve as a negative control. No significant binding of fiber head to the negative control flow cell was observed (not shown). All binding assays were carried out at 25 °C, and HBS-EP buffer (10 mM HEPES, 150 mM NaCl, 3 mM EDTA, 0.005% P20 detergent, pH 7.4) was used as running buffer. Only nontagged fiber head constructs were used in the experiments. Fiber head proteins were diluted in running buffer, and different concentrations were injected during 10 min over the CAR D1-coated surface, using a flow rate of 25 μl/min. This was followed by a wash with running buffer. The surface was regenerated with two 1-min pulses of 10 mM HCl. Primary data were fitted (with the Biaeval 3.1 software) to a "trivalent binding" model, since one trimeric fiber head can bind up to three monomeric CAR D1 molecules. This returns association rate constants in $M^{-1}\,s^{-1}$ for the first binding reaction and in $RU^{-1}\,s^{-1}$ for the second and third ones, and it is thus not possible to calculate an overall equilibrium dissociation constant (K_d) from this analysis. Therefore, equilibrium data were extracted from the sensorgrams at the end of each injection and used to calculate the K_d independently of the kinetic analysis. In the case of HAd37 fiber head constructs, whose binding to immobilized CAR is characterized by smaller constants than for CAV-2, we allowed the experiments to proceed for 15 min to obtain equilibrium data.

RESULTS

The Structure of HAd37 Fiber Head Bound to Human CAR D1 at 1.5 Å Resolution—The space group *I23* crystals contain one fiber head monomer and one CAR D1 domain per asymmetric unit. The structure was solved by molecular replacement using HAd37 fiber head and CAR D1 as search models and refined to an *R*-factor of 14.7% (*R*-free = 16.8%). Application of crystal symmetry operations to the content of the asymmetric unit results in a "triskelion" structure reminiscent of that described for the HAd12 fiber head in complex with CAR D1 (13) (Fig. 2). CAR D1 forms 15 direct hydrogen bonds with HAd37 fiber head residues in the AB loop (Asp^{191}, Ser^{193}, Gln^{200}, and Lys^{202}), β-strand B (Lys^{205}), CD loop (His^{231}), DE loop (Tyr^{266}), FG loop (Ser^{277} and Ser^{299}), and IJ loop (Glu^{351}) (Figs. 1*A* and 3). Most interacting residues are contributed by one fiber head monomer ("major binding site"), except those within the FG loop, which come from the adjacent monomer ("minor binding site"). A number of hydrophobic contacts contribute to the binding and interrupt the extensive network of bridging water molecules that fill channels and cavities between the two protein surfaces in the major site. The biggest cluster of hydrophobic residues comprises Ile^{224}, Val^{226}, Ala^{227}, Pro^{194} (HAd37 fiber head) and Leu^{58}, Leu^{73}, Val^{70}, and Val^{67} (CAR D1).

The total surface area buried upon the binding of one CAR D1 molecule by HAd37 fiber head is 2494 $Å^2$, comprising 1820 $Å^2$ for the major binding site and 674 $Å^2$ for the minor site (*i.e.* involving the FG loop from the adjacent fiber monomer). The corresponding values calculated for the HAd12-CAR D1 interface are a total of 1763 $Å^2$, comprising 1491 $Å^2$ for the major binding site and 272 $Å^2$ for the minor site (13). The HAd12-CAR D1 crystal structure revealed a poor shape complementarity of the protein-protein interface, which left cavities filled by bridging water molecules. We therefore analyzed the shape correlation statistic (S_c), a parameter that describes the shape complementarity of two protein surfaces (excluding water), which can be calculated with the program SC (63). An S_c of 1.0 represents a perfect match between the surfaces, and a value of 0.0 represents two unrelated surfaces. Typical S_c values are 0.70 – 0.76 for protease-inhibitor complexes and 0.64 – 0.68 for antibody-antigen complexes. The S_c between the surfaces of HAd37 fiber head and CAR D1 was calculated as 0.72, whereas that for HAd12-CAR D1 was 0.66. Corresponding values for the CAV-2-CAR complex are indicated below.

Superposition of the Structures of Free and CAR-bound HAd37 Fiber Heads—Comparison of HAd37 fiber head structures with and without CAR D1 (12) reveals rearrangements in the fiber head structure (root mean square (r.m.s.) deviation ($C\alpha$) = 0.6 Å), especially in the AB loop. When in complex with CAR D1, the AB loop main chain changes to adopt the M-shape typical of CAR-binding AB loops (Fig. 4*B*, compare also Fig. 4 in Ref. 10). AB loop residue Asp^{191} is flipped, and the main chain around Thr^{192} is moved by 3.3 Å toward the fiber head axis (Fig. 4*B*). This conformational change enables binding of viral Asp^{191} to Lys^{121} (CAR D1) via the side chain and to Lys^{123} (CAR D1) via the backbone oxygen (Fig. 3). It also creates space for the side chain of HAd37 Lys^{205} that now points toward the binding interface to form a hydrogen bond with Glu^{56} (CAR D1) (Fig. 4*B*). Further notable differences between CAR D1-bound and nonbound HAd37 fiber head can be found in the FG loop. FG loop residue Lys^{300} is rotated away from CAR D1, and the entire loop is shifted to avoid a steric clash between the side chain of Lys^{300} and the main chain of CAR D1 (Fig. 4*E*). The need for a conformational change in the FG loop to avoid a clash with CAR was previously pointed out from modeling studies (64). Compared with the monomeric structure of CAR D1 in solution (65), the CAR D1 C-C′ loop is shifted toward the interface between two adjacent fiber head monomers. This shift enables interactions with the FG and IJ loops of HAd37 fiber head.

The Structure of CAV-2 Fiber Head at 1.5 Å Resolution—The CAV-2 fiber head crystallized in space group $P2_1$, with two trimers per asymmetric unit. Initial phases were calculated by molecular replacement using HAd2 fiber head as a model (8) and improved by imposing the 6-fold symmetry found in the asymmetric unit. The final model has an *R*-factor of 16.5%

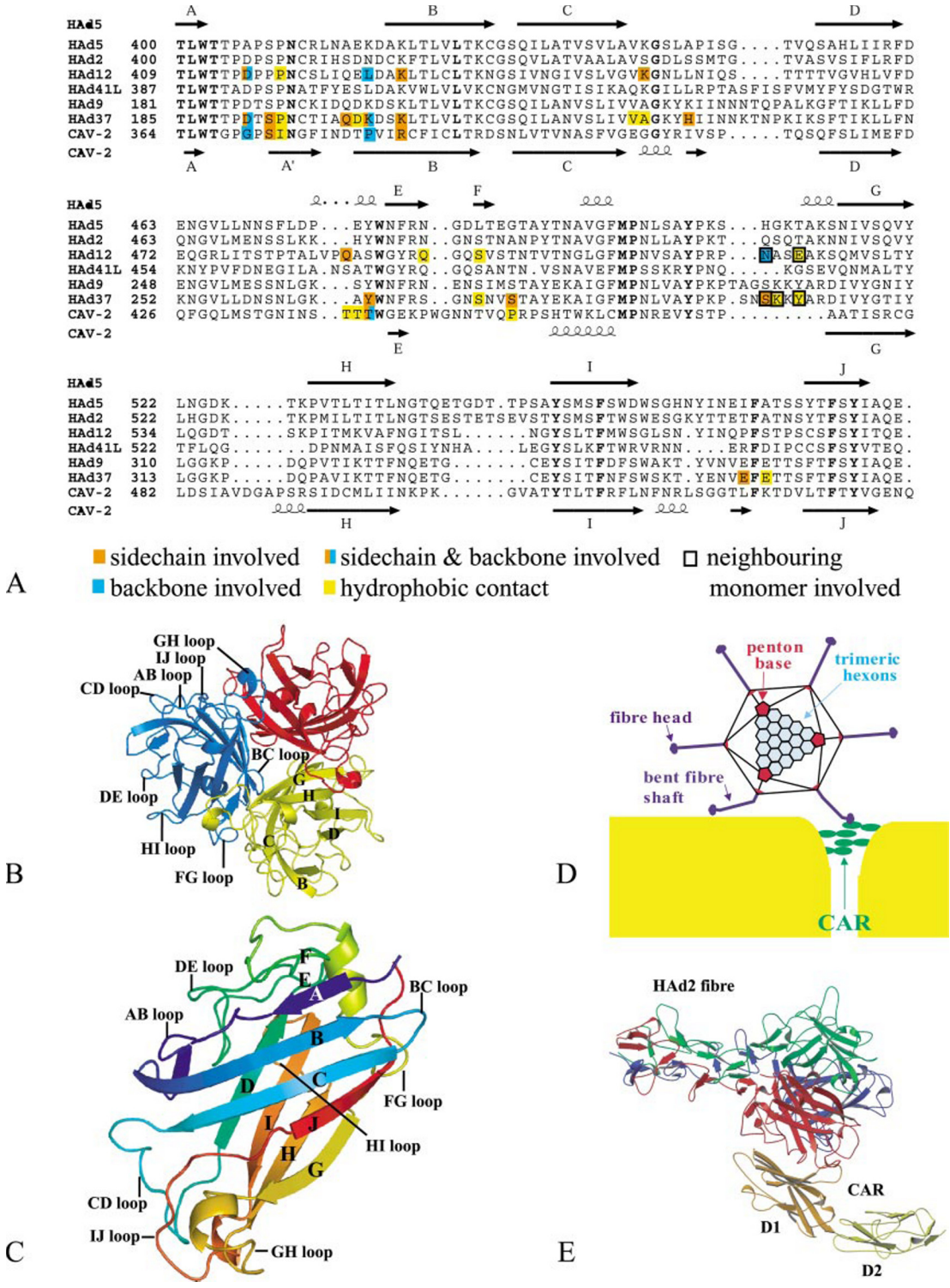

FIGURE 1. *A*, sequence alignment of adenovirus fiber heads whose CAR binding kinetics have been measured in SPR experiments (51, 67). Residues that contact CAR in crystal structures are highlighted in *different colors* to represent different types of interaction. *Orange-red*, side chain atoms of the residue are involved in contact. *Blue*, backbone atoms of the residue are involved in contact. *Half orange-red* and *half blue*, both backbone and side chain atoms are involved in contact. *Yellow*, residue is involved in a hydrophobic contact. *Black box*, the residue contributing to the interaction is located on the neighboring fiber head monomer. Residues that are conserved in all fiber head sequences aligned are shown in boldface type. *B*, *ribbon diagram* of CAV-2 fiber head trimer looking along the 3-fold axis toward the virus. The three monomers are colored *red*, *blue*, and *yellow*. Loops and visible β-strands are labeled according to the nomenclature introduced by Xia *et al.* (7). *C*, *ribbon diagram* of CAV-2 fiber head monomer, colored according to the *rainbow* from *blue* (N terminus) to *red* (C terminus). The loops and β-strands are labeled as in *B*. *D*, schematic diagram schematizing how an adenovirus might interact with CAR at tight junctions between host epithelial cells based on Refs. 31 and 38. The three major capsid proteins are indicated (hexon, penton base, and fiber). The CAR ectodomains D1 and D2 are schematized as *green ovals*. Note that CAR homodimers must dissociate for fiber binding and that the fibers of adenoviruses using CAR as a receptor contain flexible regions to permit the interaction (38). *E*, hypothetical model of HAd2 fiber (head and first part of shaft (9)) bound to CAR extracellular domains D1 and D2. The model is derived from the HAd12-CAR D1 complex (13) and the structure of the D1 + D2 domains of JAM1, the reovirus receptor, which is structurally very similar to CAR (73).

TABLE 1
Summary of crystallographic data and refinement statistics

	CAV-2 fiber head	HAd37 fiber head in complex with CAR D1	CAV-2 fiber head in complex with CAR D1
ESRF beamline	ID14-EH1	ID14-EH1	ID14-EH2
Detector	ADSC Q4R	ADSC Q4R	ADSC Q4R
Wavelength (Å)	0.934	0.934	0.933
Space group	$P2_1$	*I23*	*I422*
Cell dimensions	a = 56.1 Å, b = 88.6 Å, c = 107.2 Å, $\alpha = \gamma = 90°$, $\beta = 96.5°$	$a = b = c$ = 131.8 Å, $\alpha = \beta = \gamma = 90°$	$a = b$ = 219.9 Å, c = 387.5 Å, $\alpha = \beta = \gamma = 90°$
Resolution range (last shell) (Å)	28.4-1.5 (1.54-1.5)	29.5-1.5 (1.55-1.5)	47.7-2.3 (2.38-2.3)
Completeness (last shell)	0.95 (0.89)	0.99 (0.90)	0.96 (0.93)
R_{meas} (last shell)	0.097 (0.15)	0.06 (0.53)	0.09 (0.51)
$I/\sigma I$ (last shell)	15.3 (7.8)	25.5 (4.2)	13.4 (3.1)
R-factor (last shell)	0.165 (0.145)	0.147 (0.161)	0.172 (0.214)
R-free (last shell)	0.206 (0.207)	0.168 (0.211)	0.220 (0.295)
No. of reflections used in refinement	153,376	57,075	188,596
Fraction of reflections used for *R*-free calculation	0.02	0.05	0.01
No. of atoms (nonhydrogen)	10,007	2758	29,895
Solvent content (%)	44	53	56
Mean *B*-value	6.0	15.2	27.2
Ramachandran plot of nonglycine and nonproline residues			
Most favorable regions	806 (88%)	229 (86.1%)	2624 (85.4%)
Additional allowed regions	106 (12%)	36 (13.5%)	438 (14.3%)
Generously allowed	None	None	10 (0.3%)
Disallowed regions	None	1 (0.4%)	None
R.m.s. deviations from ideal values			
Bond distances (Å)	0.012	0.011	0.01
Angles	1.42°	1.31°	1.25°

(*R*-free = 20.6%) (Table 1). The CAV-2 fiber head is the first nonhuman fiber head structure presented so far (Fig. 1, *B* and *C*). The overall fold is close to that of known HAd fiber heads, the structurally most similar being HAd12 (r.m.s. deviation = 1.75 Å for 163 Cα positions aligned) and HAd2 (r.m.s. deviation = 1.84 Å for 160 residues aligned). A notable difference between CAV-2 fiber head and all HAd head structures determined is a short FG loop and an unusually long GH loop (12 residues compared with 7 residues in HAd12 and HAd37 fiber heads) (Fig. 1*A*). The GH loop forms a short α-helix at the top of the fiber molecule and is involved in intermonomer interactions (Fig. 1*B*).

The Structure of CAV-2 Fiber Head Bound to Human CAR D1 at 2.3 Å Resolution—The space group *I422* crystals contain four CAV-2 fiber head trimers, each bound to three CAR D1 molecules in the asymmetric unit. The structure was solved by molecular replacement using the CAV-2 fiber head and CAR D1 as search models and refined to an *R*-factor of 17.2% (*R*-free 22.0%). After refinement, *B*-values remained high for regions in CAR D1 molecules that are remote from the interface with the fiber head and that are not constrained by crystallographic contacts with neighboring molecules. For this reason, certain loop areas in these CAR D1 chains were not included in the model. The overall topology of CAV-2 fiber head bound to three CAR D1 domains is similar to that of HAd12 (13) or HAd37 fiber head in complex with CAR D1 (Fig. 2). However, each CAR D1 molecule is bound to only one CAV-2 fiber head monomer, not two as in the case of HAd12 and HAd37 (*i.e.* there is no minor binding site). As a result, CAR D1 is not packed against the cleft between two adjacent fiber head monomers (fiber head cleft) but is found in a comparably "open" conformation at the periphery of the fiber head trimer (Fig. 2). This single point of contact results in variability in the orientation of CAR D1 relative to the fiber head among the many examples in the asymmetric unit, with a maximum rotation of 5.9°. Residues forming direct hydrogen bonds with CAR D1 are located in the AB loop (Gly^{370}, Ser^{372}, and Pro^{381}), β-strand B (Arg^{384}), and the DE loop (Thr^{441}) (Figs. 2 and 3). Fixed water molecules were found within the interface between CAV-2 fiber head and CAR D1, suggesting that a water network bridging between the two protein surfaces plays an important role. Single water molecule bridges connect Gly^{406} (CAV-2) to Gln^{69} (CAR D1) and connect Glu^{405} (CAV-2) to both Val^{70} and Asp^{68} (CAR D1). Thus, fiber head regions that are not directly involved in CAR binding, such as the CD loop, contribute to CAR binding via water-mediated bonds. Residues Ile^{373} and Pro^{381} (CAV-2) and residues Leu^{73} and Val^{70} (CAR D1) form a hydrophobic patch within the interface. The FG loop does not contribute to CAR binding in a direct or water-mediated way (Fig. 4*F*).

The total surface buried upon binding of one CAR D1 to the CAV-2 fiber is 1531 $Å^2$, corresponding to just the major site. Remarkably few differences can be observed when comparing the structures of CAV-2 fiber head bound to CAR D1 and ligand-free (r.m.s. deviation (Cα) = 0.4 Å) apart from a slight movement of the AB loop about 1 Å closer to the fiber head axis (Fig. 4*C*). The calculated S_c for the interface between CAV-2 fiber head and CAR D1 is 0.55, the lowest of the three interfaces.

We note that the human and canine CAR D1 primary sequences are 94% identical (98/106 amino acids). The eight nonidentical residues are located outside the fiber-binding site, suggesting that the CAV-2 fiber head would bind the canine and human CAR D1 in an identical way.

Comparison of HAd37, HAd12, and CAV-2 Fiber Heads in Complex with Human CAR D1—Here we describe the similarities and differences between the three adenovirus fiber head CAR D1 interfaces.

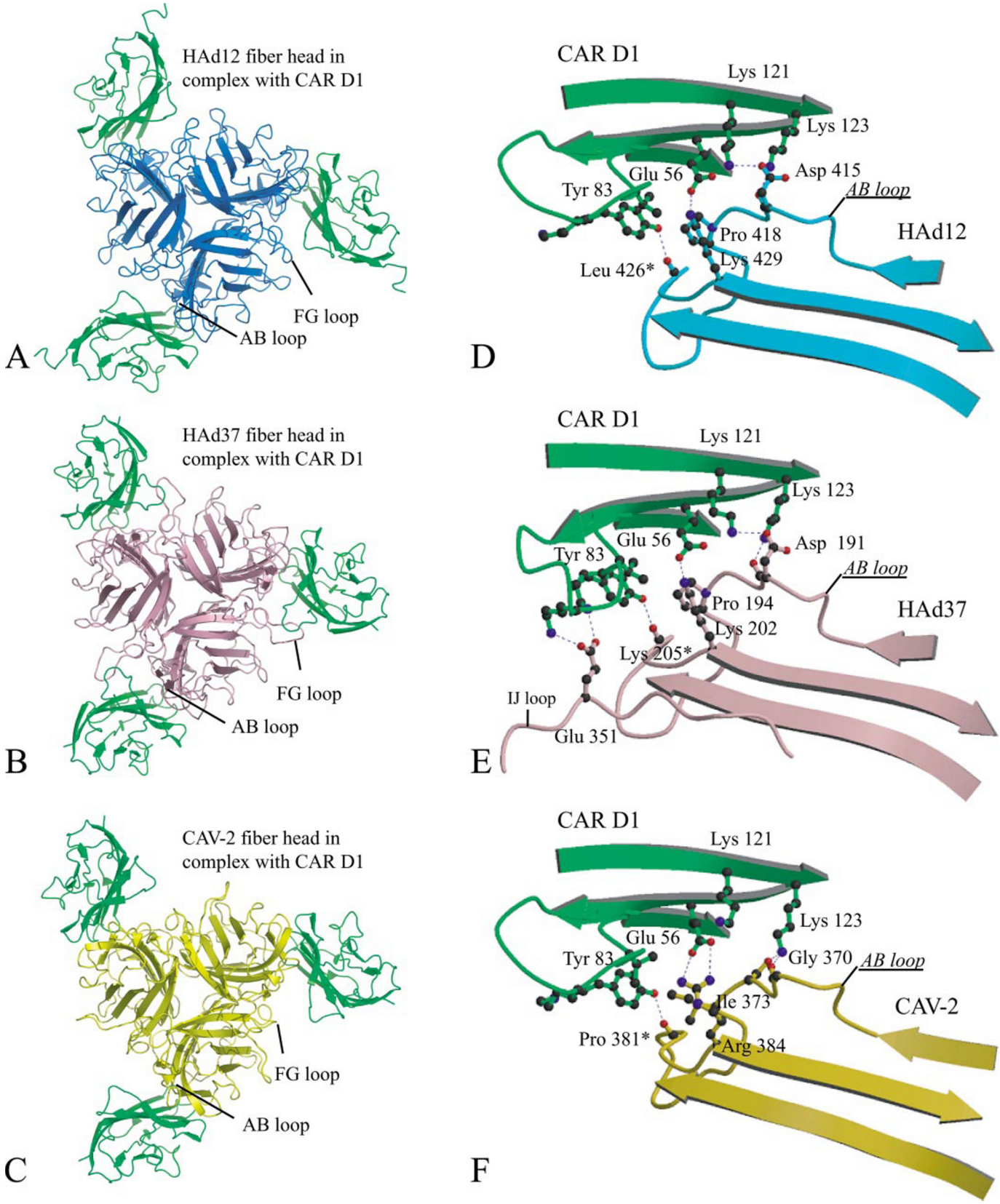

FIGURE 2. **Cartoon representations of adenovirus fiber heads in complex with CAR D1.** HAd12, HAd37, and CAV-2 fiber heads are colored *blue*, *pink*, and *yellow*, respectively. CAR D1 is in *green*. *A*, *top view* of the structure of HAd12 fiber head in complex with CAR D1 (13). *B*, as *A*, but HAd37 fiber head. *C*, as *A* and *B*, but CAV-2 fiber head. *D*, part of the binding interface between HAd12 fiber head and CAR D1 showing some key interacting residues. *E*, equivalent region of interface between HAd37 fiber head and CAR D1 showing conservation of the interactions and additional unique interactions provided by HAd37 Glu^{351} from the IJ loop. *F*, same region of the CAV-2 fiber head and CAR D1 interface showing equivalent interactions made by sometimes different fiber residues. Hydrogen bonds are shown in *dotted lines*. Residues marked with an *asterisk* are not fully represented for clarity.

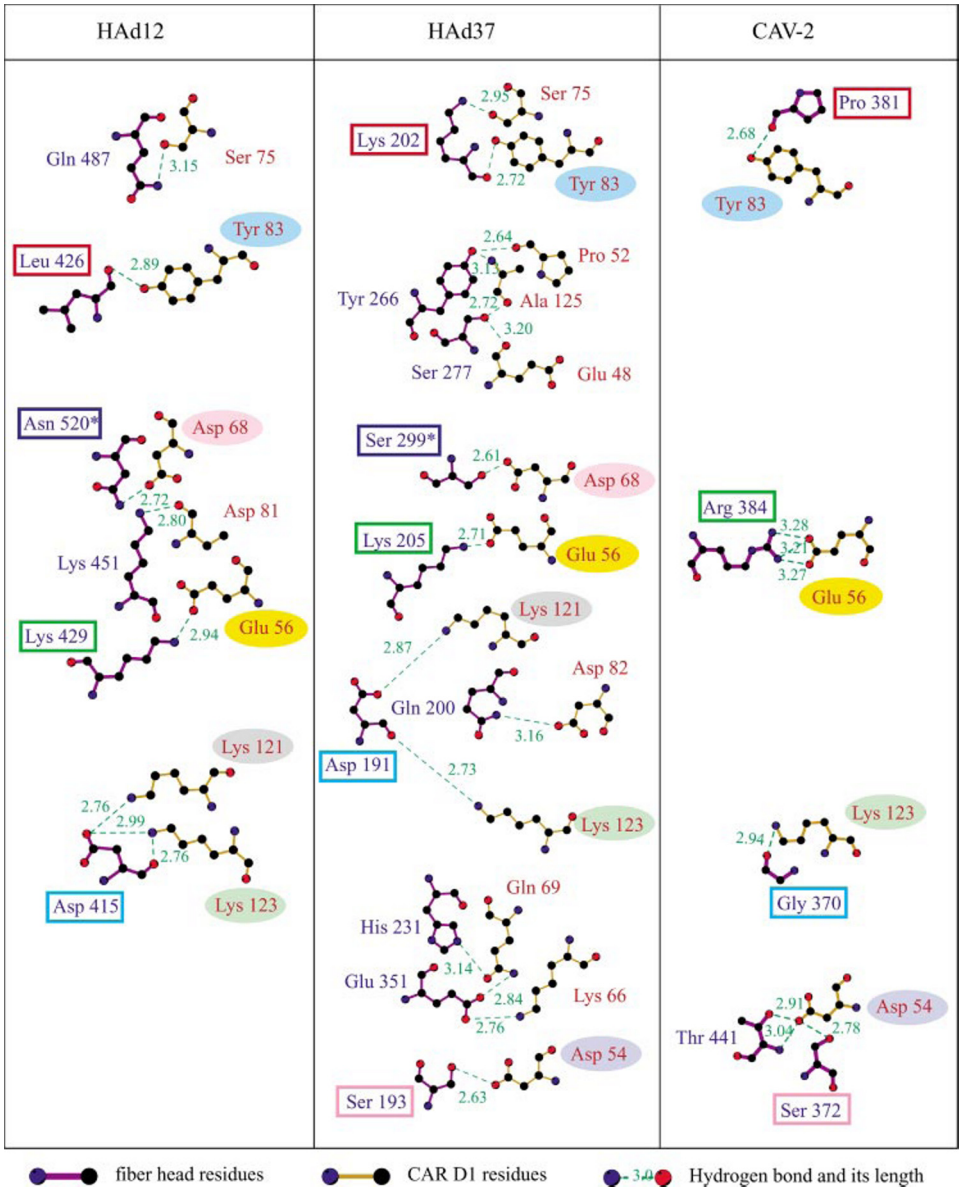

FIGURE 3. **Representation of all likely hydrogen bonds between HAd12 (13), HAd37, or CAV-2 fiber heads and CAR D1.** Carbon, oxygen, and nitrogen atoms are *black*, *red*, and *blue*, respectively. Residues involved in structurally conserved interactions are highlighted with a *colored oval* (CAR D1) or *colored box* (fiber head). Residues that contribute to the same conserved interaction in different fiber head CAR D1 complexes share the *same color* of *box* or *oval*. Residues belonging to the adjacent fiber head monomer are marked with an *asterisk*. Hydrogen bonds are represented as *dotted lines* with the crystallographically determined distance between the heavy atoms marked. The figure is derived from DIMPLOT output (62).

The Length of the FG Loop Determines the Relative Orientation of CAR D1 Relative to the Fiber Head— Superposition of the three known structures of fiber head in complex with CAR D1 shows that the orientation of CAR D1 can vary slightly. In complex with HAd12 and HAd37 fiber heads, CAR D1 is bound to two fiber head monomers simultaneously, making most contacts with one fiber head monomer (major site) and additional contacts with the FG loop of the adjacent fiber head monomer (minor site) (Fig. 4, *D* and *E*). In HAd37 fiber head, the FG loop is longer than in HAd12, and the length of the FG loop is reflected in the position of CAR D1; in complex with the HAd37 fiber head, CAR D1 is further away from the adjacent fiber head monomer than when in complex with HAd12 fiber head (Fig. 2). Interestingly, the CAR D1 C-C′ loop that binds HAd12 and HAd37 FG loops also forms hydrogen bonds with residues in the HAd37 CD and IJ loops (His^{231} and Glu^{351}). When in complex with the HAd37 fiber head, the CAR D1 C-C′ loop is shifted toward the fiber head cleft, facilitating and held in place by these additional interactions. The FG loop in CAV-2 fiber head is shortest of the three fiber heads compared and is not involved in direct contacts with CAR D1 (Fig. 4*F*). Since it is not tethered to the CAV-2 FG loop, CAR D1 is not close to the adjacent fiber head monomer (Fig. 2), and this is probably responsible for the slight flexibility in orientation observed in the crystal structure.

The AB Loop and β-Strand B Contribute to Conserved Interactions with CAR D1—It has been suggested that the most conserved fiber head region important for CAR D1 binding is the AB loop (13), and in fiber heads that do not bind CAR, this region is modified to be incompatible with CAR binding (10). The primary sequence of CAR-binding fiber heads is loosely conserved, and we find that AB loop residues from different fiber heads form equivalent contacts with the same residues in CAR D1 (HAd37 Ser^{193} and CAV-2 Ser^{372} both bind CAR D1 Asp^{54}; HAd37 Asp^{191} and HAd12 Asp^{415} both bind CAR D1 Lys^{121}) (Fig. 2, *D–F*). The strict conservation of the AB loop conformation when in complex with CAR D1 allows conserved backbone interactions with CAR D1 Lys^{123} and CAR D1 Tyr^{83}. These interactions do not depend directly on the primary AB loop sequence and are found in the three fiber head CAR D1 complexes compared (Fig. 3). A well conserved Lys (HAd12 Lys^{429}, HAd37 Lys^{205}) at the N terminus of strand B binds to the side chain of CAR D1 Glu^{56}. This Lys can be aligned to Arg^{384} in the CAV-2 fiber head, which both make a salt bridge to Glu^{56} in CAR D1 (Figs. 1*A* and 3). Hydrophobic interactions are also not strictly sequence-conserved. The hydrophobic ring of CAR D1 Tyr^{80} interacts with the side chains of AB loop residues HAd12 Leu^{426}, HAd37 Lys^{202}, and the ring of CAV-2 Pro^{381}. Also, CAR D1 Leu^{73} and Val^{70} contribute to hydrophobic centers that include the same AB loop region in all three complexes (CAV-2 Ile^{373}, HAd12 Pro^{418}, and HAd37 Pro^{194}) (Figs. 2 and 3).

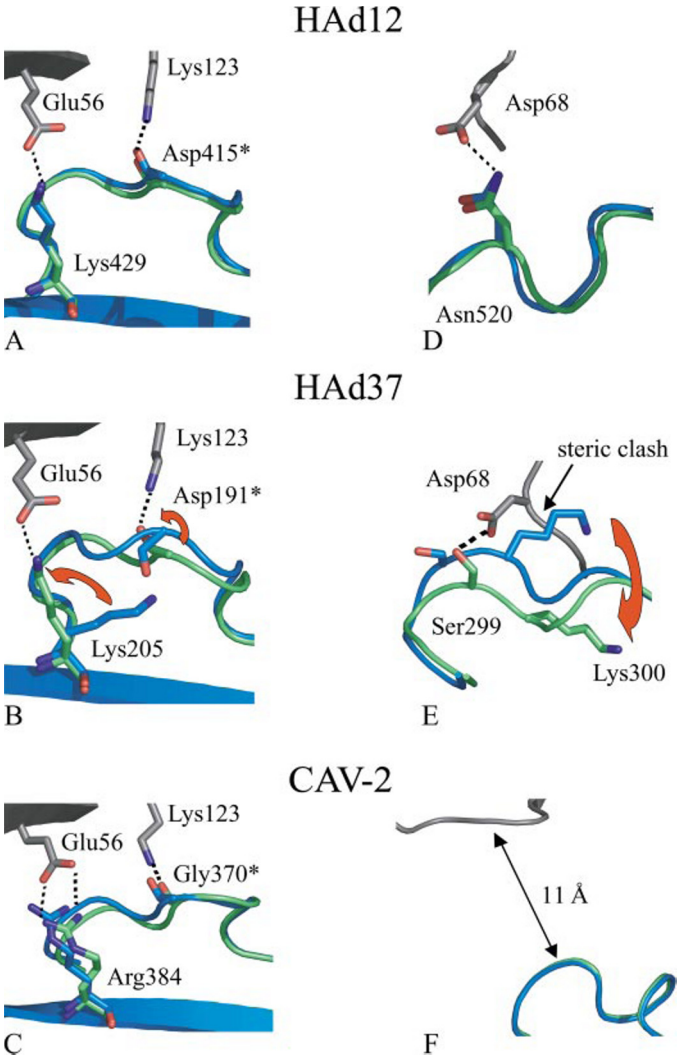

FIGURE 4. **Superposition of adenovirus fiber head AB and FG loops as found in complex with CAR D1 (*green*) or without CAR D1 (*blue*).** CAR D1 is shown in *gray*. Hydrogen bonds are shown in *dotted lines*. Differences between the CAR D1-bound and unbound forms of HAd37 fiber head loops are indicated with *red arrows*. Residues marked with an *asterisk* are not fully represented for clarity. *A*, HA12 fiber head AB loop (13); *B*, HAd37 fiber head AB loop; *C*, CAV-2 fiber head AB loop; *D*, HAd12 fiber head FG loop (13); *E*, HAd37 fiber head FG loop. Please note that the clash does not occur in reality, since the loop has a different conformation when bound to CAR D1 (shown in *green*). *F*, CAV-2 fiber head FG loop. There are no interactions between the CAV-2 fiber head FG loop and CAR D1.

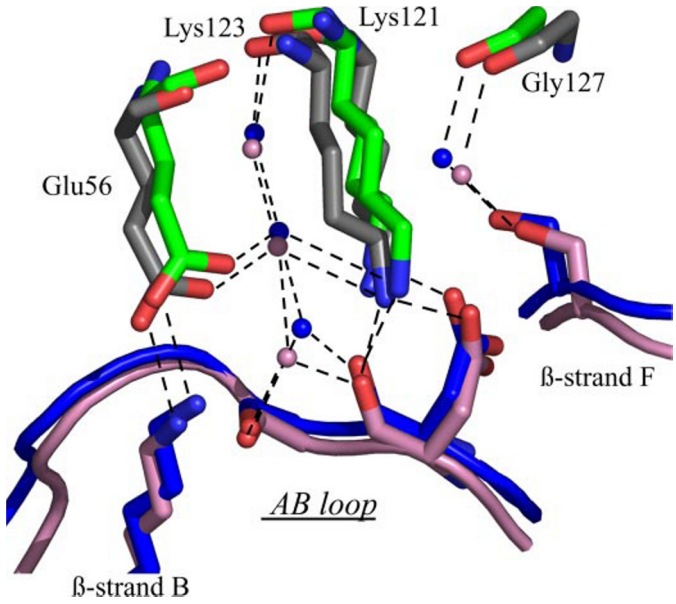

FIGURE 5. **Conserved water molecules bridging between CAR D1 (*gray* as found in complex with HAd12 fiber head (13), and *green* as found in complex with HAd37 fiber head) and the AB loops of HAd12 fiber head (*blue*) and HAd37 fiber head (*pink*).** Water molecules are represented as *spheres* that are *colored pink* in the complex with HAd37 fiber head and *blue* in the complex with HAd12 fiber head. Hydrogen bonds are represented as *dashed lines*.

Interactions Mediated by the DE Loop Are Not Conserved, although Certain Interactions Are Comparable— The primary sequence and three-dimensional structure of the DE loop is not well conserved among the three fiber heads. Although the DE loop is involved in binding CAR D1 in all structures examined, the interactions are all different. Nevertheless, it is possible to find one similarity involving HAd37 Tyr^{266} and CAV-2 Thr^{441}; these residues structurally align, and both bind to residues close to the N-terminal part of CAR D1 strand C (Pro^{52} and Asp^{54}, respectively) (Figs. 1*A* and 3).

Interactions Mediated by the CD Loop Are Not Conserved— The fiber head CD loop contacts CAR D1 differently in each of the three complexes. The HAd12 CD loop residue Lys^{451} forms a hydrogen bond with Asp^{81} in the C″-D loop of CAR D1. However, no equivalent interaction is formed by HAd37 or CAV-2 fiber heads, which contain Ala and Gly at that position (Fig. 1*A*). The HAd37 CD loop makes direct contact to the C-C′ loop of CAR D1 via a hydrogen bond between His^{231} (HAd37) and Gln^{69} (CAR D1). As mentioned previously, Gln^{69} (CAR D1) also binds to the HAd37 IJ loop (Glu^{351}), a region that is not involved in binding CAR D1 in the other two structures (Fig. 1*A*). The CAV-2 CD loop contacts CAR D1 only via water-mediated bridges (see above).

Conserved Positions for Water Molecules Bridging between Fiber Head and CAR D1—As noted in the original study of the HAd12-CAR D1 structure, water-filled cavities help glue the interface. Indeed, four of the water molecules involved in bridging between the fiber head of HAd12 and CAR D1 were found at equivalent positions in the structure of the HAd37 fiber head-CAR D1 complex (Fig. 5). Three of these connect residues in the AB loop with CAR D1 residues Lys^{121}, Lys^{123}, and Glu^{56}. A fourth water molecule forms a bridge between a conserved Ser in HAd37 or HAd12 strand F and the backbone oxygen of Gly^{127} (CAR D1) (Fig. 5). More generally, we find 11 direct bridging water molecules (*i.e.* simultaneously making a hydrogen bond to a fiber head and a CARD D1 residue) in the HAd37-CAR D1 complex major binding site but only three in the HAd12-CAR D1 complex (although it is likely that the lower resolution of this latter structure means that fewer water molecules are visible). Similarly, in the CAV-2-CAR D1 complex, there are 11 direct bridging water molecules. However, in all cases, many other ordered water molecules contribute to the networks filling the cavities.

Surface Plasmon Resonance Studies of Fiber Head CAR D1 Binding—The fiber head-CAR D1 complex structures revealed a number of interacting residues. To further investigate the importance of these interactions, we generated point mutations in HAd37 and CAV-2 fiber heads and analyzed the resulting

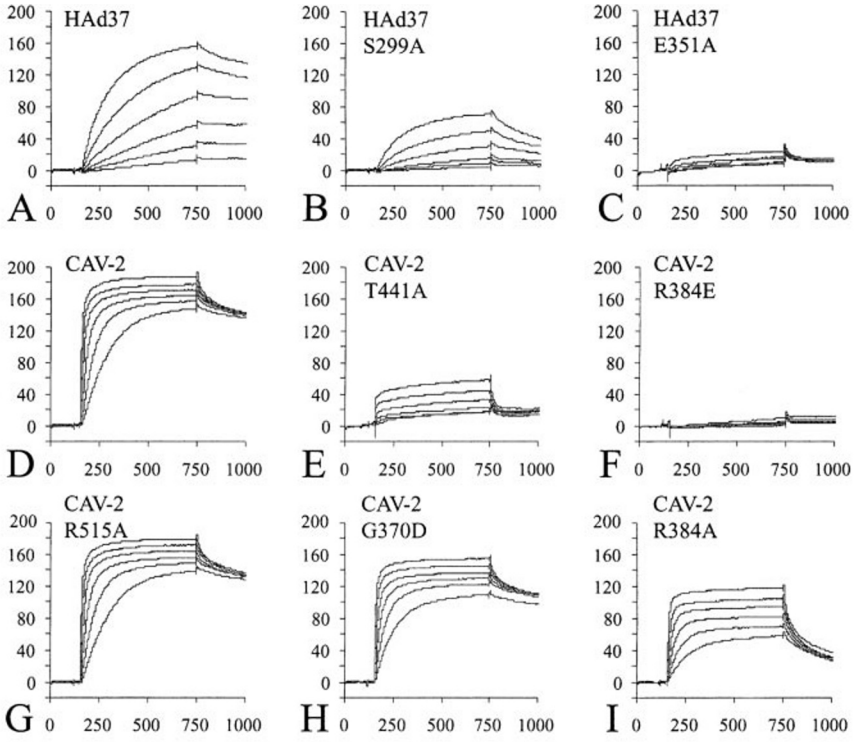

Fiber head	CAV-2$^{\alpha}$	HAd37$^{\alpha}$	HAd2$^{\beta}$	HAd5$^{\gamma}$	HAd9$^{\gamma}$	HAd12$^{\gamma}$	HAd41L$^{\gamma}$	CAV-2$^{\alpha}$ R515A	CAV-2$^{\alpha}$ G370D	CAV-2$^{\alpha}$ R384A	HAd37$^{\alpha}$ S299A
Kd	1.1 nM	20 nM	1.2 nM	7.9 nM	6.4 μM	15 nM	7.3 nM	1.2 nM	1.5 nM	4.0 nM	100 nM

FIGURE 6. **SPR sensorgrams of wild type and mutant adenovirus fiber heads binding to immobilized CAR D1.** *A*, wild type HAd37 fiber head; *B*, HAd37 fiber head mutant S299A; *C*, HAd37 fiber head mutant E351A; *D*, wild type CAV-2 fiber head; *E*, CAV-2 fiber head mutant T441A; *F*, CAV-2 fiber head mutant R384E; *G*, CAV-2 fiber head mutant R515A; *H*, CAV-2 fiber head mutant G370D; *I*, CAV-2 fiber head mutant R384A. α, results calculated from the sensorgrams. The S.E. did not exceed 15% of the K_d. β, Lortat-Jacob *et al.* (51) using the same experimental set-up and CAR construct as in this work. γ, Kirby *et al.* (67) using a longer CAR construct.

proteins for their CAR D1 binding ability using SPR. We adopted a strategy in which CAR D1 was immobilized onto the flexible dextran layer of a sensor chip, and wild type or mutant fiber heads were injected into the fluid phase over the surface. Steady-state values were extracted from the sensorgrams to calculate the equilibrium affinity (K_d) (Fig. 6).

HAd37 Fiber Head and Mutants—The HAd37 fiber head bound to CAR D1 with a K_d of 20 nM, an affinity that is 16-fold lower than that previously reported for the HAd2 fiber head-CAR D1 (51). Changing Ser^{299} (which interacts by one hydrogen bond to CAR Asp^{68} in the minor binding site) (Fig. 3) to alanine reduced the affinity to CAR D1 by 5-fold, whereas the HAd37 fiber head harboring the E351A mutation in the IJ loop lost CAR D1 binding entirely, highlighting the importance of the two strong hydrogen bonds mediated by this residue (Fig. 3).

CAV-2 Fiber Head and Mutants—The CAV-2 fiber head bound CAR DI with an affinity of about 1 nM, which together with the value for HAd2, is the highest among those measured by SPR (Fig. 6). However, using a fluorescence anisotropy binding assay in solution (66), we found that the CAV-2 fiber knob bound CAR D1 with an affinity that was 2.5-fold higher than HAd2 (data not shown). In the case of the CAV-2 mutants, an R384A mutation, which would eliminate the prominent salt bridge with Glu^{56} (Fig. 3), only reduced the affinity 4-fold, whereas the charge reversal mutation R384E abolished measurable CAR D1 binding. A large negative effect on binding was found with the mutation T441A (at the beginning of strand E; see Fig. 1*A*), probably due to the weakening or disruption of the three hydrogen bonds involving CAR D1 Asp^{54} (Fig. 3). In the AB loop, we replaced Gly^{370} by an Asp that occurs in many other fiber heads at this position (Fig. 1*A*). We expected that this might enhance the binding due to extra hydrogen bonding opportunities. However, we found that there was no notable affect on the affinity to CAR D1. As a control, we also made a change distant from the CAR binding site, R515A, which displayed similar binding kinetics to the wild type.

These results highlight the fact that it is difficult to predict from structural data the contribution(s) that interface interactions make to the affinity. In addition, they show that idiosyncratic (*i.e.* serotype-specific) interactions (*e.g.* that of Glu^{351} of HAd37 or Thr^{441} of CAV-2) can have a greater significance than, for instance, the conserved salt bridge with CAR D1 Glu^{56}.

DISCUSSION

We have presented the crystal structure of CAV-2 fiber head at 1.5 Å resolution and found, as expected, that it is very similar to that of HAd fiber heads. We also solved the crystal structures of CAV-2 and HAd37 fiber heads in complex with their receptor CAR D1 at 2.3 and 1.5 Å resolution, respectively (Fig. 2). We compared these two new complex structures with that at 2.6 Å resolution HAd12 fiber head in complex with CAR D1 (13). We then introduced point mutations to CAV-2 and HAd37 fiber heads to study by surface plasmon resonance binding assays the contribution of selected residues to CAR binding (Fig. 6).

Current structure-based understanding of the fiber-CAR interaction is mainly based on the only existing complex structure, that of HAd12 and CAR D1 (13). This pioneering study highlighted the importance of the AB loop in the direct interactions between CAR and fiber head but also noted that the interface showed unexpectedly poor shape complementarity, despite the complex being of high affinity. The authors explained this contradiction by the fact that ordered water molecules trapped in the cavities between the two surfaces could act as a molecular glue, cross-linking the proteins by hydrogen bonding. Furthermore, they proposed that such a partially water-mediated interaction would permit greater freedom to

the virus to maintain receptor binding specificity while altering its sequence in response to immune pressure. In a subsequent study, mutations were made in the HAd12 fiber head to make it more like that of HAd2, which was determined by a fluorescence binding assay to have an 8-fold higher affinity for CAR D1 than HAd12 (66). Structures were determined at 3.3 and 2.9 Å resolution of the P417S and S489Y mutants, respectively, of HAd12 fiber head in complex with CAR D1. These supported the idea that the increased affinity of HAd2 to CAR was probably due to additional hydrogen bonds across the interface, although the relatively low resolution did not allow a detailed analysis of the effect on the water structure. Mutational studies of the fiber-CAR interaction have also been made on other serotypes (reviewed in Ref. 64), the general conclusion being that whereas some interactions seem to be conserved, there is considerable variability in which residues are involved. This modulates the affinity by about 10-fold, with the exception of HAd9 fiber head that has an exceptionally low affinity to CAR (67).

Our analysis of the now available fiber head CAR D1 complex structures reveals that three elements are common to the CAR-binding sites examined as follows. 1) The overall triskelion topology of the three Ad fiber head CAR D1 complexes is similar (Fig. 2). 2) The M-shaped main-chain conformation of the AB loop is conserved and critically allows the formation of hydrophobic interactions with CAR D1 and two conserved hydrogen bonds between backbone carbonyl oxygen atoms and CAR D1 residues Tyr^{83} and Lys^{123} (Figs. 2 and 3). 3) A conserved interaction is formed between a positively charged residue in strand B (Lys or Arg) with CAR D1 residue Glu^{56}. However, this interaction is not essential in the case of CAV-2 fiber head, since the R384A mutation reduces the affinity for CAR D1 only 4-fold (Fig. 6).

On the other hand, five notable differences were found between the three complexes. 1) CAR D1 contacts two neighboring fiber head monomers in the complexes with the human Ad fiber heads but only one in the CAV-2 complex, due to the shortness of the FG loop (Fig. 2). 2) The number of residues involved in binding CAR D1, the amount of surface buried, and the surface complementarity at the binding interface differ significantly between the three fiber heads. Comparative total buried surface area, number of direct hydrogen bonds between residues, and shape complementarity are 2494 $Å^2$ (1675 major, 674 minor), 15 hydrogen bonds, and $S_c = 0.72$ for HAd37; 1763 $Å^2$ (1491 major, 272 minor), 8 hydrogen bonds, and $S_c = 0.66$ for HAd12; and 1531 $Å^2$ (all major, no minor), 7 hydrogen bonds, and $S_c = 0.55$ for CAV-2. Surprisingly, the interface with the most shape complementarity and largest number of interactions, that between HAd37 fiber head and CAR D1 (Fig. 3), has the lowest affinity (see below) and *vice versa* for CAV-2. 3) The IJ loop of the fiber head is essential for CAR D1 complex formation with HAd37 fiber head (since the E351A mutation abolishes binding) but is not involved in HAd12 and CAV-2 CAR-binding (Fig. 6). 4) HAd37 fiber head undergoes significant conformational changes to bind CAR D1, but HAd12 and CAV-2 fiber heads do not (Fig. 4). 5) The K_d of purified fiber head to immobilized human CAR D1 varies between about 1 and 20 nM among most serotypes tested with SPR, the highest and lowest affinities being for CAV-2 and HAd37 fiber heads, respectively (summarized in Fig. 6). HAd9 has an exceptionally high K_d of 6.4 μm (67).

These results confirm and extend the previous observations discussed above concerning the unusual nature of the adenovirus fiber-CAR interaction, compared with other virus-receptor interactions. The fiber head-CAR D1 interface is of relatively poor shape complementarity, allowing it to tolerate significant variation in the identity of residues involved in direct contact while preserving high affinity. This is in contrast to the "canyon hypothesis," proposed on the basis of studies of rhinovirus and its receptor (ICAM1) (68), which postulated that key receptor binding residues would be within narrow surface depressions and hence inaccessible to antibodies, thus allowing them to be highly conserved.

This and previous studies, show that the structural basis for the unique adenovirus fiber-CAR interaction is a conserved core interaction between CAR and the AB loop region of the fiber head combined with variable additional interactions. This interaction depends critically on the M-shaped main-chain conformation of the AB loop, which should carry in its N-terminal part (following the TLWT motif) only small, polar or nonpolar, (Gly, Ala, Pro, Ser, Thr, and Asp). Interestingly, the non-CAR binding HAd3 and HAd41 short fiber heads violate these two conditions (10). The CAR compatible AB loop allows the formation of hydrophobic side-chain interactions with CAR D1, two hydrogen bonds between fiber head backbone carbonyl oxygen atoms and CAR D1 residues Tyr^{83} and Lys^{123} (and sometimes Lys^{121} as well), and a salt bridge with Glu^{56} of CAR D1 (Fig. 2). A network of ordered water molecules that make further bridging interactions reinforces this core interaction (Fig. 5). Other interactions, particularly with various loops of the fiber head, are serotype-specific but can nevertheless make a significant contribution to the binding affinity.

The tolerance to mutation of the fiber head-CAR D1 interaction is clearly of selective value to the virus in escaping host immune response surveillance. Two mechanisms seem to play a role in the conservation of the CAR binding specificity of the fiber head, despite random mutations. First, the AB loop region is tolerant to restricted mutations that preserve the core hydrophobic and polar interactions, and second, novel interactions can be introduced involving other loops while losing unrelated contact points. In this way, the strength of the interaction with CAR can be maintained, although it may modulate in response to other factors related to the particular tropism of different serotypes. It is important to note that the degree of conservation does not necessarily correlate with the importance of an interaction. Thus, the nonconserved bond between the HAd37 IJ loop and CAR D1 is essential for CAR-binding, whereas the functionally conserved bond between CAV-2 Arg^{384} and CAR D1 is not (Fig. 6).

Although HAd37 fiber head makes numerous contacts with CAR D1, the overall affinity is lower than that found for CAV-2 (Fig. 6). As mentioned above, this highlights the fact that it is extremely difficult to predict from structural data the contribution(s) that interface interactions make to the affinity. A possible explanation in this case is the fact that only HAd37 fiber head needs to undergo conformational changes to bind CAR

D1, notably in the AB and FG loop regions (Fig. 4). These changes probably have a free energy cost that is only partially offset by the binding energy, thus resulting in a relatively low affinity. The reduced affinity between HAd37 fiber head and CAR D1 may also reflect that this interaction is not required for initial binding to the cell yet has been preserved for another biological function, possibly to aid virus escape.

All three fiber heads compared here bind CAR D1; however, only HAd12 and CAV-2 use CAR as a receptor. It has been proposed that geometrical aspects of the relative orientation of fiber and CAR and the length of the fiber shaft play a role *in vivo*. First, CAR is located on the basolateral side of epithelial cells and not easily accessible (26). Second, it has been argued that the need for the virus to be able to bind CAR and cellular integrins simultaneously necessitates a long and flexible fiber shaft as found in HAd12 but not in HAd37 (38). CAV-2 has a relatively long fiber shaft (about 35 nm) consisting of at least 18 repeats, and it contains a flexible region allowing the fiber to bend close to the middle of the fiber shaft.[6] We also suggest that the low number of direct contact points and absence of binding to the adjacent monomer results in a more flexible CAV-2-CAR D1 complex, adding to the effect of the flexible shaft. In fact, the relative orientation of CAV-2 fiber head and CAR D1 molecules toward each differs by up to 5.9° in our crystal structure, supporting this hypothesis. In contrast, HAd37 fiber head provides a larger binding interface and over 20 contact points with CAR D1, giving a relatively rigid complex that in fact is unable to form in the context of the virion at the cell surface.

Both CAV-2 virions (46) and chimeric HAd5 viruses with subgroup D fibers (*e.g.* from HAd37 (69)) or CAV-2 fiber heads (70) are being developed as gene transfer vectors. The design of such vectors is greatly aided by structural understanding of the fiber and interactions with cellular ligands. In particular, more specific vector targeting may be achieved by modification of these interactions. One way to do this rationally is by designing point mutants that disrupt undesired binding to certain receptors and promote the binding to others. To this end, elimination of CAR binding by HAd5 fiber has already been achieved (71, 72). In this work, we identify point mutants of CAV-2 and HAd37 fiber heads with greatly reduced ability to bind immobilized CAR D1. Notably, CAV-2 fiber head mutant R384E does not bind CAR D1 at all, and mutations T441A and R384A have reduced affinity. Similarly, we constructed a HAd37 fiber head mutant, E351A, which does not bind CAR D1, and another, S299A, that binds CAR with a 5-fold lower affinity (Fig. 6).

Our crystallographic and biochemical results have provided detailed insight into adenovirus interaction with CAR and how it is conserved despite sequence variation and led to the design of mutations that eliminate CAR binding. These findings will contribute to the development of Ad gene transfer vectors.

Acknowledgments—We are grateful to European Synchrotron Radiation Facility and EMBL staff for help on the synchrotron beamlines and to Chloe Zubieta for data collection on the CAV-2 fiber head crystals.

[6] G. Schoehn, E. Seiradake, H. Lortat-Jacob, O. Billet, E. J. Kremer, and S. Cusack, unpublished observations.

REFERENCES

1. Benko, M., and Harrach, B. (2003) *Curr. Top. Microbiol. Immunol.* **272,** 3–35
2. Kojaoghlanian, T., Flomenberg, P., and Horwitz, M. S. (2003) *Rev. Med. Virol.* **13,** 155–171
3. Chakrabarti, S., Mautner, V., Osman, H., Collingham, K. E., Fegan, C. D., Klapper, P. E., Moss, P. A., and Milligan, D. W. (2002) *Blood* **100,** 1619–1627
4. Rux, J. J., and Burnett, R. M. (2000) *Mol. Ther.* **1,** 18–30
5. Rux, J. J., Kuser, P. R., and Burnett, R. M. (2003) *J. Virol.* **77,** 9553–9566
6. Zubieta, C., Schoehn, G., Chroboczek, J., and Cusack, S. (2005) *Mol. Cell* **17,** 121–135
7. Xia, D., Henry, L. J., Gerard, R. D., and Deisenhofer, J. (1994) *Structure* **2,** 1259–1270
8. van Raaij, M. J., Louis, N., Chroboczek, J., and Cusack, S. (1999) *Virology* **262,** 333–343
9. van Raaij, M. J., Mitraki, A., Lavigne, G., and Cusack, S. (1999) *Nature* **401,** 935–938
10. Seiradake, E., and Cusack, S. (2005) *J. Virol.* **79,** 14088–14094
11. Durmort, C., Stehlin, C., Schoehn, G., Mitraki, A., Drouet, E., Cusack, S., and Burmeister, W. P. (2001) *Virology* **285,** 302–312
12. Burmeister, W. P., Guilligay, D., Cusack, S., Wadell, G., and Arnberg, N. (2004) *J. Virol.* **78,** 7727–7736
13. Bewley, M. C., Springer, K., Zhang, Y. B., Freimuth, P., and Flanagan, J. M. (1999) *Science* **286,** 1579–1583
14. Cusack, S. (2005) *Curr. Opin. Struct. Biol.* **15,** 237–243
15. Fabry, C. M., Rosa-Calatrava, M., Conway, J. F., Zubieta, C., Cusack, S., Ruigrok, R. W., and Schoehn, G. (2005) *EMBO J.* **24,** 1645–1654
16. Saban, S. D., Nepomuceno, R. R., Gritton, L. D., Nemerow, G. R., and Stewart, P. L. (2005) *J. Mol. Biol.* **349,** 526–537
17. Abrescia, N. G., Cockburn, J. J., Grimes, J. M., Sutton, G. C., Diprose, J. M., Butcher, S. J., Fuller, S. D., San Martin, C., Burnett, R. M., Stuart, D. I., Bamford, D. H., and Bamford, J. K. (2004) *Nature* **432,** 68–74
18. Benson, S. D., Bamford, J. K., Bamford, D. H., and Burnett, R. M. (1999) *Cell* **98,** 825–833
19. Benson, S. D., Bamford, J. K., Bamford, D. H., and Burnett, R. M. (2004) *Mol. Cell* **16,** 673–685
20. Wickham, T. J., Mathias, P., Cheresh, D. A., and Nemerow, G. R. (1993) *Cell* **73,** 309–319
21. Albinsson, B., and Kidd, A. H. (1999) *Virus Res.* **64,** 125–136
22. Soudais, C., Boutin, S., Hong, S. S., Chillon, M., Danos, O., Bergelson, J. M., Boulanger, P., and Kremer, E. J. (2000) *J. Virol.* **74,** 10639–10649
23. Chillon, M., and Kremer, E. J. (2001) *Hum. Gene Ther.* **12,** 1815–1823
24. Bergelson, J. M., Cunningham, J. A., Droguett, G., Kurt-Jones, E. A., Krithivas, A., Hong, J. S., Horwitz, M. S., Crowell, R. L., and Finberg, R. W. (1997) *Science* **275,** 1320–1323
25. Tomko, R. P., Xu, R., and Philipson, L. (1997) *Proc. Natl. Acad. Sci. U. S. A.* **94,** 3352–3356
26. Cohen, C. J., Shieh, J. T., Pickles, R. J., Okegawa, T., Hsieh, J. T., and Bergelson, J. M. (2001) *Proc. Natl. Acad. Sci. U. S. A.* **98,** 15191–15196
27. Roelvink, P. W., Lizonova, A., Lee, J. G., Li, Y., Bergelson, J. M., Finberg, R. W., Brough, D. E., Kovesdi, I., and Wickham, T. J. (1998) *J. Virol.* **72,** 7909–7915
28. Honda, T., Saitoh, H., Masuko, M., Katagiri-Abe, T., Tominaga, K., Kozakai, I., Kobayashi, K., Kumanishi, T., Watanabe, Y. G., Odani, S., and Kuwano, R. (2000) *Brain Res. Mol. Brain Res.* **77,** 19–28
29. Raschperger, E., Thyberg, J., Pettersson, S., Philipson, L., Fuxe, J., and Pettersson, R. F. (2006) *Exp. Cell Res.* **312,** 1566–1580
30. van Raaij, M. J., Chouin, E., van der Zandt, H., Bergelson, J. M., and Cusack, S. (2000) *Struct. Fold Des.* **8,** 1147–1155
31. Walters, R. W., Freimuth, P., Moninger, T. O., Ganske, I., Zabner, J., and Welsh, M. J. (2002) *Cell* **110,** 789–799
32. Arnberg, N., Edlund, K., Kidd, A. H., and Wadell, G. (2000) *J. Virol.* **74,** 42–48
33. Gaggar, A., Shayakhmetov, D. M., and Lieber, A. (2003) *Nat. Med.* **9,** 1408–1412

34. Segerman, A., Arnberg, N., Erikson, A., Lindman, K., and Wadell, G. (2003) *J. Virol.* **77,** 1157–1162
35. Sirena, D., Lilienfeld, B., Eisenhut, M., Kalin, S., Boucke, K., Beerli, R. R., Vogt, L., Ruedl, C., Bachmann, M. F., Greber, U. F., and Hemmi, S. (2004) *J. Virol.* **78,** 4454–4462
36. Wu, E., Trauger, S. A., Pache, L., Mullen, T. M., von Seggern, D. J., Siuzdak, G., and Nemerow, G. R. (2004) *J. Virol.* **78,** 3897–3905
37. Wu, E., Fernandez, J., Fleck, S. K., Von Seggern, D. J., Huang, S., and Nemerow, G. R. (2001) *Virology* **279,** 78–89
38. Wu, E., Pache, L., Von Seggern, D. J., Mullen, T. M., Mikyas, Y., Stewart, P. L., and Nemerow, G. R. (2003) *J. Virol.* **77,** 7225–7235
39. Shayakhmetov, D. M., and Lieber, A. (2000) *J. Virol.* **74,** 10274–10286
40. Both, G. W. (2002) in *Adenoviral Vectors for Gene Therapy* (Curiel, D., and Douglas, J., eds) pp. 447–479, Academic Press, Inc., San Diego
41. Paillard, F. (1997) *Hum. Gene Ther.* **8,** 2007–2009
42. Klonjkowski, B., Gilardi-Hebenstreit, P., Hadchouel, J., Randrianarison, V., Boutin, S., Yeh, P., Perricaudet, M., and Kremer, E. J. (1997) *Hum. Gene Ther.* **8,** 2103–2115
43. Kremer, E. J. (2004) *J. Gene Med.* **6,** Suppl. 1, 139–151
44. Kremer, E. J., Boutin, S., Chillon, M., and Danos, O. (2000) *J. Virol.* **74,** 505–512
45. Soudais, C., Laplace-Builhe, C., Kissa, K., and Kremer, E. J. (2001) *FASEB J.* **15,** 2283–2285
46. Soudais, C., Skander, N., and Kremer, E. J. (2004) *FASEB J.* **18,** 391–393
47. Amalfitano, A., and Parks, R. J. (2002) *Curr. Gene Ther.* **2,** 111–133
48. Keriel, A., René, C., Galer, C., Zabner, J., and Kremer, E. J. (2005) *J. Virol.* **80,** 1487–1496
49. Kremer, E. J. (2005) *Curr. Genomics* **6,** 13–39
50. Neufeld, E. F. (1991) *Annu. Rev. Biochem.* **60,** 257–280
51. Lortat-Jacob, H., Chouin, E., Cusack, S., and van Raaij, M. J. (2001) *J. Biol. Chem.* **276,** 9009–9015
52. Kabsch, W. (1988) *J. Appl. Crystallogr.* **21,** 916–924
53. McCoy, A. J., Grosse-Kunstleve, R. W., Storoni, L. C., and Read, R. J. (2005) *Acta Crystallogr. Sect. D Biol. Crystallogr.* **61,** 458–464
54. Leslie, A. G. (1999) *Acta Crystallogr. Sect. D Biol. Crystallogr.* **55,** 1696–1702
55. Terwilliger, T. C. (2003) *Acta Crystallogr. Sect. D Biol. Crystallogr.* **59,** 38–44
56. Iwase, K., and Hirono, S. (1999) *J. Comput. Aided Mol. Des.* **13,** 499–512
57. Collaborative Computational Project 4 (1994) *Acta Crystallogr. D Biol. Crystallogr.* **50,** 760–763
58. Perrakis, A., Morris, R., and Lamzin, V. S. (1999) *Nat. Struct. Biol.* **6,** 458–463
59. Murshudov, G. N., Vagin, A. A., Lebedev, A., Wilson, K. S., and Dodson, E. J. (1999) *Acta. Crystallogr. Sect. D Biol. Crystallogr.* **55,** 247–255
60. Emsley, P., and Cowtan, K. (2004) *Acta Crystallogr. Sect. D Biol. Crystallogr.* **60,** 2126–2132
61. Laskowski, R. A., MacArthur, M. W., Moss, D. S., and Thornton, J. M. (1993) *J. Appl. Crystallogr.* **26,** 283–291
62. Wallace, A. C., Laskowski, R. A., and Thornton, J. M. (1995) *Protein Eng.* **8,** 127–134
63. Lawrence, M. C., and Colman, P. M. (1993) *J. Mol. Biol.* **234,** 946–950
64. Law, L. K., and Davidson, B. L. (2005) *Mol. Ther.* **12,** 599–609
65. Jiang, S., Jacobs, A., Laue, T. M., and Caffrey, M. (2004) *Biochemistry* **43,** 1847–1853
66. Howitt, J., Bewley, M. C., Graziano, V., Flanagan, J. M., and Freimuth, P. (2003) *J. Biol. Chem.* **278,** 26208–26215
67. Kirby, I., Lord, R., Davison, E., Wickham, T. J., Roelvink, P. W., Kovesdi, I., Sutton, B. J., and Santis, G. (2001) *J. Virol.* **75,** 7210–7214
68. Rossmann, M. G. (1989) *J. Biol. Chem.* **264,** 14587–14590
69. Denby, L., Work, L. M., Graham, D., Hsu, C., von Seggern, D. J., Nicklin, S. A., and Baker, A. H. (2004) *Hum. Gene Ther.* **15,** 1054–1064
70. Glasgow, J. N., Kremer, E. J., Hemminki, A., Siegal, G. P., Douglas, J. T., and Curiel, D. T. (2004) *Virology* **324,** 103–116
71. Roelvink, P. W., Mi Lee, G., Einfeld, D. A., Kovesdi, I., and Wickham, T. J. (1999) *Science* **286,** 1568–1571
72. Leissner, P., Legrand, V., Schlesinger, Y., Hadji, D. A., van Raaij, M., Cusack, S., Pavirani, A., and Mehtali, M. (2001) *Gene Ther.* **8,** 49–57
73. Prota, A. E., Campbell, J. A., Schelling, P., Forrest, J. C., Watson, M. J., Peters, T. R., Aurrand-Lions, M., Imhof, B. A., Dermody, T. S., and Stehle, T. (2003) *Proc. Natl. Acad. Sci. U. S. A.* **100,** 5366–5371